International Journal of Biological Macromolecules 231 (2023) 123297

Contents lists available at ScienceDirect

International Journal of Biological Macromolecules

journal homepage: www.elsevier.com/locate/ijbiomac

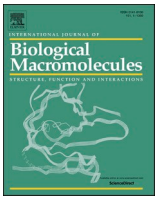

Electro-stimulated drug release by methacrylated hyaluronic acid-based conductive hydrogel with enhanced mechanical properties

Didem Aycan, Fatma Karaca, Atıf Koca, Neslihan Alemdar *

Marmara University, Department of Chemical Engineering, Istanbul, Turkey

ARTICLE INFO

Keywords:
Hyaluronic acid
Electro-stimulated release
Ibuprofen

ABSTRACT

Recently, the design of stimuli-responsive hydrogels for controlled drug delivery systems has been extensively investigated to meet therapeutic needs and optimize the release pattern of the drug. Being a natural polyelectrolyte, hyaluronic acid (HA) is excellent potential to generate new opportunities for electro-responsive drug carrier applications. In the current study, HA-based electroconductive hydrogel was developed as a novel smart drug carrier for anti-inflammatory drug release by the combination of in-situ and post polymerization mechanisms. HA was modified through methacrylation reaction to introduce photocrosslinkable groups into its structure and then reduced graphene oxide (rGO) was encapsulated into methacrylated HA (HA/MA) hydrogel by using the photopolymerization technique. In the post polymerization process, polyaniline (PANI) was incorporated/loaded into HA/MA-rGO polymeric network produced in previous step. The produced HA/MA-rGO-PANI hydrogel exhibited sufficient electrical conductivity providing the desirable electro-responsive ability for Ibuprofen (IBU) release. Furthermore, it has superior mechanical performance compared to pure (HA/MA) and rGO containing (HA/MA-rGO) hydrogels. IBU release from the hydrogel was successfully triggered by electrical stimulation and the cumulative drug release also enhanced by increasing of the applied voltage. These results highlighted that the novel HA/MA-rGO-PANI hydrogel could be a promising candidate for electrical-stimulated anti-inflammatory release systems in neural implant applications.

1. Introduction

Stimuli-responsive drug delivery systems, which have the ability to react against internal or external triggers (i.e. pH, light, magnetic or electric field, temperature, etc.), have emerged as an attractive approach to enhance efficacy and spatial/temporal control of the drug release as well as to provide compliance and comfort to patients [1–5]. Since these systems can modify drug release behaviors in accordance with the therapeutic needs by responding to changes in physiological conditions, they become prominent as a more favorable and beneficial option over the conventional ones. Among the various types of stimuli, electrical stimuli have gained much attention in triggered drug delivery due to ensuring an easy and inexpensive route for adjusting and controlling drug release by generating accurate signals [6–9]. Therefore, electrical stimuli materials can be utilized as promising drug delivery platforms for on-demand and transdermal systems and implants [10]. Particularly, delivery of the drugs such as anti-inflammatory reagents from neural implants via electrical stimulation has become a remarkable field in the last decades [10–13] since the release of the anti-inflammatory drugs from the implant into the tissue surrounding by using this strategy offers promoted tissue integration, enhanced performance stability of the implants and reduction of biotic reactions and inflammatory response [14–17].

In order to develop the electro-responsive drug carrier with superior features for neural implants, hydrogels are commonly used as an excellent class of materials because (i) their hydrophilic and soft nature are similar to the biological tissues, (ii) their porous 3D structure of them makes easier to load drug molecules into hydrogel matrix and (iii) their high water content could promote the biocompatibility and offer an ion-rich physiological medium [18–21]. Compared with the hydrogels produced by using synthetic polymers, natural polymers, especially polysaccharide (chitosan, dextran, hyaluronic acid (HA), etc.) based hydrogels are more advantageous owing to their biodegradability, non-toxicity and biocompatibility characteristics in practical applications of drug delivery [22–26]. Despite these brilliant features, hydrogels generally suffer from insufficient mechanical performance and electrical conductivity which are the critical requirements for electrical-stimuli systems [2,5,27,28]. Electroconductive hydrogels (ECHs), which are

* Corresponding author at: Marmara University, Department of Chemical Engineering, 34854 Istanbul, Turkey.
E-mail addresses: didem.aycan@marmara.edu.tr (D. Aycan), neslihan.alemdar@marmara.edu.tr (N. Alemdar).

https://doi.org/10.1016/j.ijbiomac.2023.123297
Received 11 September 2022; Received in revised form 17 December 2022; Accepted 12 January 2023
Available online 14 January 2023

typically fabricated by either in-situ polymerization in the presence of conductive particles or using post polymerization of intrinsically conductive polymers (CPs), have been widely studied in order to eliminate the mentioned drawbacks [29]. Conductive particles (carbon nanotubes, nanoparticles and graphene-family materials) are incorporated into the prepolymer solution to form ECH by in-situ polymerization process. Since this method does not require extra steps to eliminate cytotoxic oxidants or byproducts, ECHs produced with this strategy could be directly used in bio-related applications without purification [30,31]. In particular, graphene oxide (GO) and reduced graphene oxide (rGO) have received a great deal of attention in the production of ECHs by this method. Their unique physical and chemical properties, large surface area, mechanical strength and high electron mobility inspire the researchers to develop new concepts for developing ECH networks, which would be employed as an electro-responsive drug carrier for proposed applications [32–34].

In order to fabricate ECH, post polymerization is another technique that involves the immersion of a preformed hydrogel network to the monomer solution of the conductive polymer. In the ECHs produced by this method, while the hydrogel component of the ECH enables to carry a higher amount of drug molecules, the sufficient electroactivity of the CPs could assist to regulate electrically-triggered cellular activities and cellular performance that makes these materials potential candidates for drug delivery in neural implants [35–38]. Moreover, the integration of CPs such as polyaniline (PANI), polypyrrole (PPy) and poly (3,4-ethylenedioxythiophene) (PEDOT) with hydrogel network allows the controlled drug delivery by way of oxidation or reduction mechanisms thanks to their unique redox behavior [20,25,39,40]. PANI is one of the most attractive CPs and it exhibits excellent properties like tunable electrical conductivity, flexibility, environmental and thermal stability, acceptable biocompatibility, protonation/deprotonation ability and easy and facile synthesis. Owing to all its superior advantages, PANI has been extensively used in the regeneration of various types of natural tissues (nerve, bone, cardiac, muscle etc.) and is preferred for the production of ECH-based drug delivery systems [41–45].

Herein, we aimed that the production of methacrylated HA (HA/MA)-based ECH as an electro-responsive drug carrier by the combination of in-situ polymerization and post polymerization in the presence of rGO and PANI, respectively to benefit from the advantages of these different fabrication strategies and each component of the hydrogel network. HA, a natural-origin polysaccharide, was selected as the main component of the hydrogel network [46–48] because it plays the main structural role in the extracellular matrix (ECM) with its similar characteristics to biological tissues that resulted in the extensive usage of HA for various biomaterial applications [49–51]. Furthermore, the polyelectrolyte characteristic of the HA is very favorable for electrically stimulated systems [52]. In order to form HA/MA-based electroconductive hydrogel network, three main steps were performed (i) HA being functional groups was modified by integrating methacrylate groups into its backbone via an esterification reaction. (ii) rGO was introduced into the polymeric structure by the photopolymerization technique which is the most favorable and easiest method to fabricate hydrogels with tunable and consistent chemical and physical characteristics, as well as high reproducibility. Furthermore, photocrosslinking offers significant advantages like in-situ gelation, spatio-temporal control of hydrogel network, minimal energy requirement and absence of volatile organic substances over the conventional crosslinking methods. (iii) PANI was formed/loaded into the hydrogel network which was produced in the previous step.

At this point, it is worth mentioning that the current study carried out on the fabrication of ECH for the electric-response drug release is to bring a novel approach to the literature in terms of not only the usage of HA/MA-based hydrogel but also the combination of two production methods (in-situ and post polymerization) via different conductivity sources.

The produced hydrogels by this new formulation were evaluated regarding their chemical structures, morphologies, thermal and swelling behavior, electrical and mechanical properties. The obtained results clearly revealed that the introduction of both rGO and PANI as the different conductivity sources into the hydrogel network not only improved the electrical conductivity providing the desirable electro-responsive ability for controlled drug release but also enabled superior mechanical performance to produced hydrogels compared to their single usage. To investigate passive and electric-driven drug release behaviors of the HA/MA-rGO-PANI hydrogel, Ibuprofen (IBU) was used as a model drug because it prevents the inflammatory reactions between the neural implants and tissues, which suppresses cell proliferation and differentiation [10,53,54]. The release measurements exhibited that a higher amount of cumulative drug release by electrical stimulation compared to passive drug release were achieved by this formulation. Furthermore, the obtained "on-off" drug release pattern also confirmed that the hydrogel could release more amount of drug due to the application of voltage and fewer amount of drug was released from the hydrogel without any voltage enforcement. Consequently, it could be stated that the fabricated HA/MA-rGO-PANI hydrogel with a natural-origin structure that possesses sufficient electroconductivity and mechanical performance could be employed as an electro-responsive drug carrier to release anti-inflammatory reagents from the neural implants in order to diminish the neuroinflammatory response in further applications.

2. Materials and methodology

2.1. Materials

Hyaluronic acid (HA, food grade, Mw = 8×10^5 Da) was provided from Heze Better Biochemical Co. (Shandong, China). Ethanol (EtOH), sodium hydroxide (NaOH), ammonium peroxodisulfate (APS) and aniline ($C_6H_5NH_2$) were purchased from Merck. Methacrylic anhydride (MA), photoinitiator (Irgacure 2959, 2-Hydroxy-4′-(2-hydroxyethoxy)-2-methylpropiophenone), phosphate buffer saline (PBS) tablet, graphite (powder $<$ 20 μm, synthetic), hydrazine (35 wt% in H_2O), methanol (MeOH) and 12–14 kDa cutoff dialysis tubing were obtained from Sigma Aldrich. IBU was kindly provided from Bilim Pharmaceuticals, Turkey. All chemicals were used as received without further purification. Cell culture solution including Dulbecco's Modified Eagle Medium (DMEM) was purchased from GIBCO, USA. The medium formulation was supplemented with Fetal bovine serum (FBS) (GIBCO, USA) and penicillin/streptomycin/amphotericin (PSA) (GIBCO, USA). 3-(4,5-di-methylthiazol-2-yl)-5-(3-carboxy-methoxy-phenyl)-2-(4-sulfophenyl)-2H-tetrazolium (MTS assay) was provided from Promega, Southampton, UK.

2.2. Synthesis of rGO

rGO was synthesized by the chemical reduction of graphene oxide (GO), which was produced from graphite following the modified Hummer's method [55–57]. For the reduction, hydrazine was added into the aqueous dispersion of GO as a reducing agent under continuous stirring at 100 °C for 24 h. After cooling down, the obtained rGO solution was centrifuged followed by the washing process with methanol and distilled water, subsequently. In the final step, the filtrate was kept at room temperature under vacuum for 72 h.

2.3. Synthesis of methacrylated HA (HA/MA)

Firstly, 1 g of HA was dissolved in distilled water until complete dissolution. After that, 4.8 ml of MA was slowly added into the solution under continuous stirring at 4 °C. The pH was maintained at 8 with 6 N NaOH solution and the reaction was carried out at 4 °C for 24 h in the dark. The obtained HA/MA was precipitated in EtOH. The product was filtered, washed and dissolved, followed by dialysis against deionized water for 4 days. Purified HA/MA was freeze-dried and stored at 4 °C for

further use.

2.4. Synthesis of HA/MA-rGO hydrogel by in-situ polymerization

HA/MA (10 mg) was dissolved in PBS (1 ml) overnight under continuous stirring. The photoinitiator (2-Hydroxy-4′-(2-hydroxyethoxy)-2-methylpropiophenone) (0.5 w/v) was added into the solution and stirred until fully dissolved. Firstly, to form pure HA/MA hydrogel, prepolymer (HA/MA) solution without rGO was injected to the round-glass mold and exposed to UV light irradiation (365 nm) for 30 min. Secondly, the stock rGO suspension was prepared in EtOH (1 % w/v) by ultrasonic treatment for 20 min. Then, the optimized amount of suspension (3 % w/w) was added into prepolymer (HA/MA) solution. This mixture was exposed to UV light with molds for 30 min in the presence of a photoinitiator to obtain HA/MA-rGO hydrogel.

2.5. Synthesis of HA/MA-rGO-PANI hydrogel by post polymerization

The obtained HA/MA-rGO hydrogels were immersed into ANI monomer solution (0.08 M) and incubated for 12 h at room temperature. An equimolar amount of APS (0.08 M) was added into the solution as an initiator and the reaction was carried out for 3 h. After that, hydrogels were immersed into distilled water for washing process and incubated for 2 days at room temperature. The washing procedure was continued until obtaining a clear solution. In the final step, produced HA/MA-rGO-PANI hydrogels were dried in petri dishes overnight at room temperature.

2.6. Characterization

The chemical structures of GO, rGO, HA, HA/MA and the produced hydrogels were determined by Fourier transform infrared spectroscopy (FT-IR). FT-IR spectroscopy was performed using a Perkin Elmer Spectrum One FT-IR with attenuated total (ATR) unit. The samples were scanned from 380 to 4000 cm^{-1}. The methacrylation degree of HA/MA was analyzed by proton nuclear magnetic resonance spectroscopy (^{1}H NMR). The ^{1}H NMR spectra were recorded on a 500 MHz Varian Unity Inova NMR at 25 °C using deuterium oxide (D_2O) as the solvent. GO and rGO were also characterized with Raman spectroscopy that was recorded with a STEX-100 Compact Confocal Raman spectrometer with a laser at 532 nm as the excitation source in order to evaluate the reduction efficiency. The particle size of rGO dispersions was measured by a Zetasizer Nano ZS (Malvern Instruments, Malvern, UK) at the scattering angle θ = 173°, and the temperature was fixed at 25 °C. The surface morphologies of the hydrogels sputter coated with Au/Pd were investigated using scanning electron microscopy (SEM) (ZEISS EVO MA10).

2.7. Swelling properties

The swelling capacity of the hydrogels was evaluated gravimetrically. The dry weights (W_d) of the hydrogels were measured. Then, dry hydrogels were incubated in PBS (pH = 7.4) at 37 °C for 24 h. The swollen hydrogels were blotted to remove superficial liquids and swollen weights (W_s) of the hydrogels were measured. The swelling capacity of the hydrogels was calculated according to Eq. (1):

$$Swelling\ capacity\ (\%) = \frac{W_s - W_d}{W_d} * 100 \quad (1)$$

2.8. Thermal behavior

In order to observe thermal stability of the hydrogels, thermogravimetric analysis (TGA) was performed by "Netzsch STA 449 F3 Jupiter" thermogravimetric apparatus in the temperature range of 25 °C and 900 °C with a heating rate of 20 K/min. Argon was used as the carrier gas.

2.9. Electrical conductivity

The electrical conductivity of the hydrogels was measured by using Lucas Labs S-302 Four Point Resistivity Probing Equipment, which has four equally spaced metallic probes touched to the material surface, connected to a Gamry Instruments power source. The sheet resistance (ρ) is determined by supplying a constant current between outer probes and monitoring the voltage between inner probes [55] and it is calculated by using Eq. (2). Each sample was tested three times.

$$\rho = 2\pi sR \quad (2)$$

where s is the probe spacing, R is the measured resistance value.

Then, the conductivity value (σ) of the hydrogels was calculated by using the determined sheet resistivity according to Eq. (3):

$$\sigma = \frac{1}{\rho} \quad (3)$$

2.10. Mechanical performance

In order to examine the mechanical properties of the produced hydrogels prepared in cylindrical form, the compressive stress-strain measurements were carried out with a Universal Testing Machine (Zwick Roell- Z1.0 Mechanical Test Machine) at the 2 mm/min of crosshead speed. Elastic modulus of the hydrogels was determined from the stress-strain curves and compressive strength values were calculated by using Eq. (4):

$$CS = \frac{F_{max}}{A} \quad (4)$$

where F_{max} corresponds to the maximum force (N), A represents the cross-sectional area of the sample (mm^2).

Each composition was tested in triplicate and average values were recorded for the accuracy.

2.11. In vitro degradation study

In vitro degradation test of HA/MA-rGO-PANI hydrogel was carried out in PBS solution (pH 7.4) for 7 days. Dry hydrogels with approximately 5.0 mg of weight were immersed into a falcon tube containing 10 ml of PBS solution and were incubated at 37 °C. At predetermined time intervals, hydrogels were taken out from the degradation solution, washed thoroughly with distilled water and following that, they were dried at 37 °C. The in vitro degradation profile of HA/MA-rGO-PANI hydrogel was determined by measuring the weight loss (%) of samples at each predetermined time interval, as calculated in Eq. (5):

$$Weight\ loss\ (\%) = \frac{W_I - W_{II}}{W_I} \quad (5)$$

where W_I and W_{II} are the weight of the dry hydrogel before and after degradation at each predetermined time intervals, respectively.

2.12. Cytotoxicity test

The cytotoxicity of the HA/MA-rGO-PANI hydrogel was determined by using the viability assay. Briefly, HaCaT cells were seeded onto the 96-well plates with regular cell culture media (DMEM-LG containing 10 % FBS and 1 % PSA) containing HA/MA-rGO-PANI hydrogel and media only at a density of 5×10^3/well and incubated for 24 h. Following incubation, the cell viability was measured by a colorimetric MTS assay (#G3582, CellTiter 96 Aqueous One Solution). Each well was treated with 10 % MTS reagent prepared in the culture media. The plates were incubated in a humidified chamber (5 % CO_2, 80 % RH, and 37 °C) for 1

h in the dark. Absorbance values of the end-products of the reaction were determined by a plate reader (ELx800, Biotek Instruments, USA) at 490 nm wavelength. Lastly, cells incubated with the HA/MA-rGO-PANI hydrogel were compared with the ones treated with medium only and the results were analyzed accordingly.

2.13. Passive and electric-driven drug release study

For passive drug release experiments, hydrogels were loaded with model drug (IBU) through the incubation in stock drug solution for 24 h at 37 °C and after that, they were washed with distilled water in order to remove the weakly bonded drug on hydrogels' surface. Then, drug loaded hydrogels immersed in falcon tubes with 10 ml of PBS (pH 7.4) were placed into the incubator at 37 °C, 130 rpm to simulate the physiological environment. 1 ml of release solution was withdrawn at specific time intervals and replaced with the same amount of fresh PBS solution to provide a constant volume release medium. The amount of IBU released from the hydrogels was observed by using UV–Vis spectrophotometry at the wavelength of 265 nm. The drug loading capacity of the hydrogels was calculated according to Eq. (6):

$$\textit{Drug loading capacity}\ (\%) = \frac{W_2 - W_1}{W_1} \times 100 \quad (6)$$

where W_1 and W_2 are the weight of the hydrogel and the weight of the drug loaded hydrogel, respectively.

Electric-driven drug release experiments were carried out by employing a three-electrode system placed in 20 ml of PBS at 37 °C. While the fabricated HA/MA-rGO-PANI electroconductive hydrogel was used as the working electrode, platinum (Pt) mesh and silver/silver chloride (Ag/AgCl) electrodes were used as counter and reference electrodes, respectively. The release of the drug was triggered by applying different voltage values (0 V, 1 V and 3 V) to examine the effect of applied voltage on the release characteristics of the hydrogels. Additionally, on-off pulse release was tested under 3 V of potential for 3 min at 30 min intervals. The same procedure carried out for passive drug release was also performed for the stimulated-drug release to determine the cumulative drug release.

2.14. Statistical analysis

GraphPad Prism Software (V.5, San Diego, USA) was used for statistical analysis. One way ANOVA was performed for a comparison test. The results were presented as means ± standard deviation (SD) within the 95 % confidence level.

3. Results and discussions

3.1. Synthesis and characterization of rGO

To investigate the structural characterization of graphite, GO and rGO, FT-IR and RAMAN analyses were performed. As seen from the Fig. 1A, although the FT-IR spectrum of graphite did not show any peaks corresponded to the presence of oxygen-containing functional groups, the peaks appeared in the FT-IR spectrum of GO at 1708 (C═O stretching vibrations), 1163 (C-O-C stretching vibrations) and, 1038 cm^{-1} (C—O stretching vibrations) which are characteristic for GO, confirm that the oxygen functionalized groups were successfully introduced to the graphite structure after the oxidation process [58–61]. Additionally, the absorption band at 3114 cm^{-1} is assigned to the O—H stretching vibration for GO [59,62]. The bands at 2815 and 2900 cm^{-1} could be attributed to symmetric and asymmetric stretching vibrations

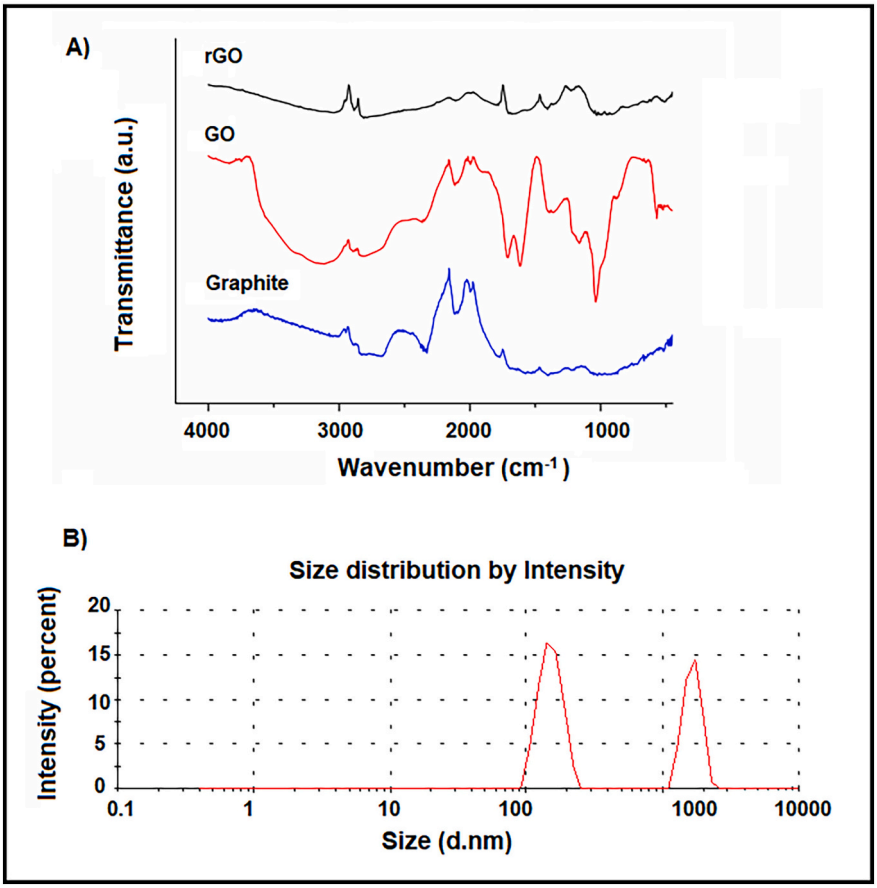

Fig. 1. FT-IR spectra (A) of graphite, GO and rGO and particle size distribution (B) of rGO.

of CH_2. Furthermore, the sharp peak at 1618 cm^{-1} resulted from the hydrogen bonds between graphite and water molecules, which approves the hydrophilic nature of the GO [63]. The reduction was confirmed by removing and decreasing the peaks related to oxygen-containing groups in the FT-IR spectrum of rGO [64,65]. While the peaks corresponding to C-O-C and C═O stretching almost disappeared, the peaks refer to C—O stretching decreased dramatically for rGO sample. Moreover, the decreases in the hydroxyl group region (3000–3500 cm^{-1}) are another evidence of the reduction process. The decrease of oxygen-containing groups rather than their total elimination during reduction shows that residual oxygen functionalities remain still in the rGO structure [66,67]. Raman analysis, a favored tool for characterizing graphene-family materials, was also performed to confirm the oxidation and reduction processes. The ratio of the peak intensity of D-band to that of G-band (I_D/I_G) indicated the disorder degree of the carbonaceous materials were calculated for graphite, GO and rGO. As shown in Table 1, I_D/I_G value increased after the oxidation that was arisen from the formed disordered structure related to the presence of oxygen-containing functional groups in GO. Besides, the increased intensity ratio after the reduction suggested the creation of a more isolated graphitic domain in the rGO structure due to the removal of functional groups from the latter form. These consistent results obviously showed that GO and rGO were synthesized successfully.

The obtained rGO particle size distribution was determined using a particle size analyzer (Fig. 1B). According to the measurements, the average particle size was found as 2.2 μm, which provided a good dispersion of rGO in a polymeric mixture.

3.2. Synthesis and characterization of HA/MA

In order to achieve photo-induced crosslinking, HA was methacrylated through an esterification reaction, which occurred by the chemical displacement of primary and secondary hydroxyl groups of HA with methacrylate groups (Scheme 1).

The methacrylation of HA was confirmed by FT-IR spectroscopy. As shown in Fig. 2A, the FT-IR spectra of both HA and HA/MA exhibited the characteristic peaks at about 3300, 2900, 1600 and 1400 cm^{-1}, indicating O—H and N—H stretching, C—H stretching, C═O asymmetric stretching and C—H bending vibrations, respectively. A strong absorption band was observed at about 1040 cm^{-1} in both spectra, corresponding to the presence of C-O-C bending [68,69]. In the FT-IR spectrum of HA/MA, the bands appearing at 1716 cm^{-1} and 1449 cm^{-1} depicted C═O (carbonyl) stretching and C═C (carbon-carbon double bonds) of conjugated system, respectively [70]. The presence of these bands confirmed the successfully insertion of methacrylate groups into the HA backbone.

The reaction between HA and MA was also proved by ^1H NMR analyses and the related spectrum was depicted in Fig. 2B. The characteristic peaks appeared at 5.80 and 6.20 ppm were assigned to the $=CH_2$ protons of methacrylate groups. The peaks from 1.88 to 1.98 ppm ascribed to methyl resonance that indicates that methacrylate moiety conjugated to HA successfully [71–73]. The degree of methacrylation was calculated as 19 % based on integrating the relevant NMR peaks.

3.3. Fabrication and characterization of electroconductive hydrogels

HA/MA based ECHs were synthesized through the combination of the in-situ polymerization and post polymerization methods, as demonstrated in Scheme 2. The plausible chemical interactions between the components of the hydrogel network were also depicted in Scheme 3.

While the color of the pure HA/MA hydrogel was transparent, the color of rGO containing hydrogel was light grey. After post polymerization, the color of the hydrogel turned from light grey to dark green proving that PANI was successfully loaded/formed in the hydrogel network.

For the characterization of chemical structures, HA/MA, HA/MA-rGO and HA/MA-rGO-PANI hydrogels were compared to each other by using FT-IR analysis. As seen in Fig. 3, the FT-IR spectrum of HA/MA-rGO possessed not only the characteristic peaks corresponding to HA/MA as explained above in detail but also the peaks due to the incorporation of rGO, which were nearly in the same region with pure hydrogel. The decreasing of the intensities and the slight shifting of the peaks for the bands at about 1070, 1400 and 1700 cm^{-1} compared to pure HA/MA hydrogel also indicated the hydrogen bonding between oxygen containing groups of rGO and C═O (carbonyl) groups of HA/MA [74]. In the spectrum of HA/MA-rGO-PANI hydrogel, the characteristic peaks of PANI also appeared at 1558, 1487 and 1238 cm^{-1} corresponding to stretching vibrations of quinone ring, benzenoid ring and C—N stretching vibration of secondary amine, respectively, as well as characteristic peaks of HA/MA-rGO structure. The band at 801 cm^{-1} was for out-of-plane bending of 1,4-disubstituted benzene. Additionally, absorption bands at about 3000 and 2330 cm^{-1} were attributed to N—H and O=C-O stretching vibrations of PANI [75–77].

The morphologies of produced HA/MA, HA/MA-rGO and HA/MA-rGO-PANI hydrogels were investigated by SEM analysis (Fig. 4). The polymeric network morphology was observed in the SEM image of HA/MA hydrogel [78]. The incorporation of rGO created the interconnected porous structure that resulted in the formation of open channels for the migration of molecules [78,79]. Therefore, it could be stated that the presence of rGO improved the permeability of the hydrogel, which was consistent with the swelling test results [80]. It could also be noticed that the layered structure of rGO was observed in the polymeric network without any agglomeration proved the homogenous distribution of rGO in the hydrogel structure. When the SEM image of HA/MA-rGO-PANI hydrogel was examined, it was clearly seen that the hydrogel surface was covered with the polymeric PANI spheres that is similar to the studies reported in the literature [81–83]. The possible reason for the formation of these spherical structures after the addition of PANI could be attributed to the dispersion forces resulted from the hydrophobic nature of PANI molecules [84]. As also shown in Fig. 4C, these PANI spheres stuck with each other due to the strong hydrogen bonding between PANI and the polymeric network, which is considered as the driving force for the self-assembly of PANI spheres resulted in a phase-separated morphology [83,85]. Since these PANI spheres were partially filled the pores of the hydrogel network, the water uptake capacity of the hydrogel was consistently reduced. This morphology could be also provided an advantage in the electrical conductivity by creating the continuous electron transfer pathway [86].

3.4. Thermal behavior

Thermal stabilities of HA/MA, HA/MA-rGO and HA/MA-rGO-PANI hydrogels were presented by TGA and DTG results (Fig. 5). All TGA curves, whose decomposition peaks were made explicit in DTG curves, indicated that weight loss of the hydrogels occurred in three main steps. The first weight loss for HA/MA hydrogel with a maximum decomposition rate at 151 °C was assigned to the removal of residual water molecules, which bound to carboxylate groups by polar interactions [87]. While the second weight loss occurred between 185 and 335 °C due to the decomposition of organic components, the third one was observed between 340 and 390 °C as the main decomposition of polymeric side chains. The TGA curve of HA/MA-rGO demonstrated similar degradation patterns to HA/MA hydrogel except for slight peak shifting and peak broadening for the first degradation step owing to oxygen-containing functional groups coming from the rGO structure.

Table 1
The relative intensity ratio values of graphite, GO and rGO.

	Graphite	GO	rGO
I_D/I_G	0.27	0.79	1.10

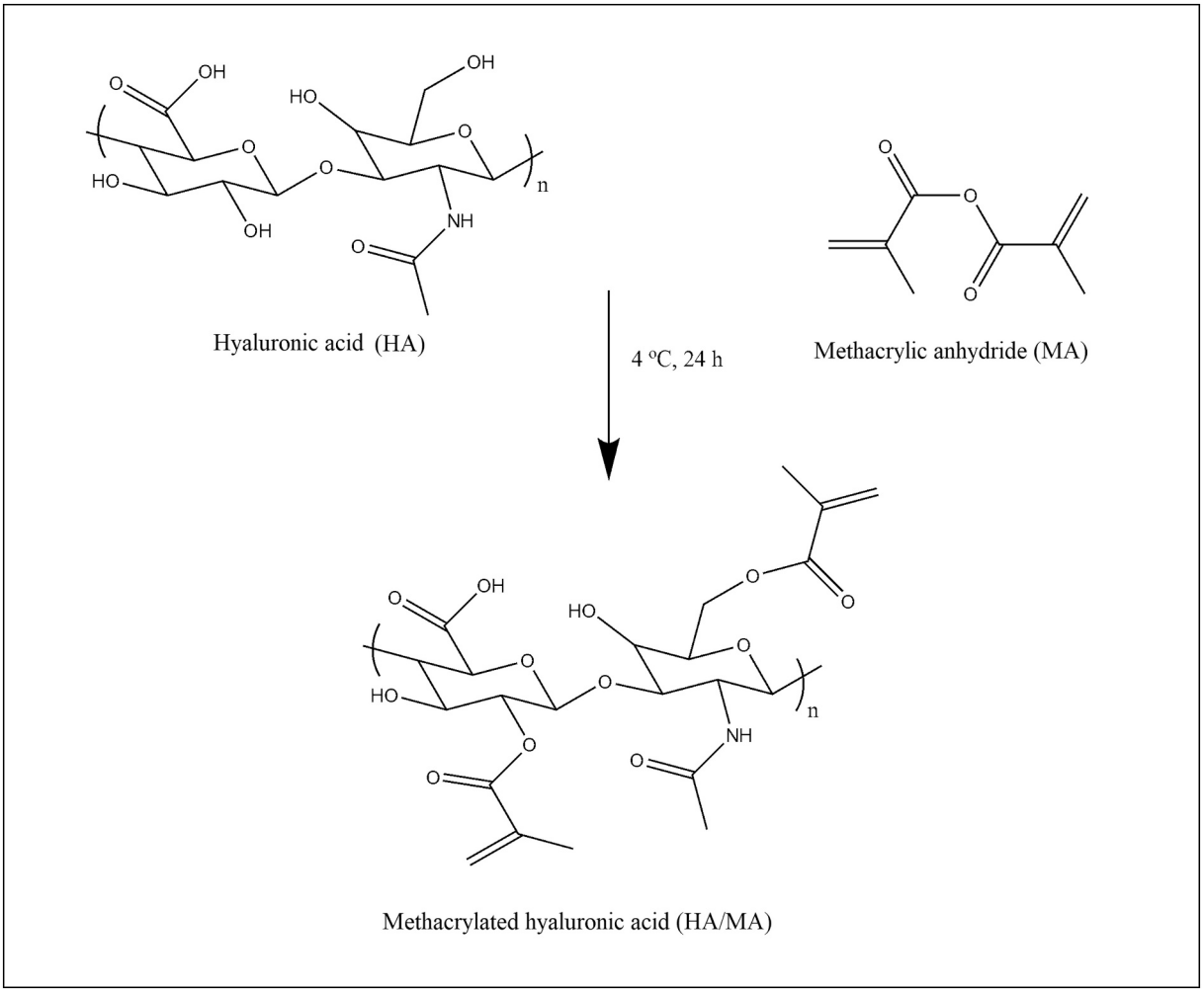

Scheme 1. Synthesis of HA/MA.

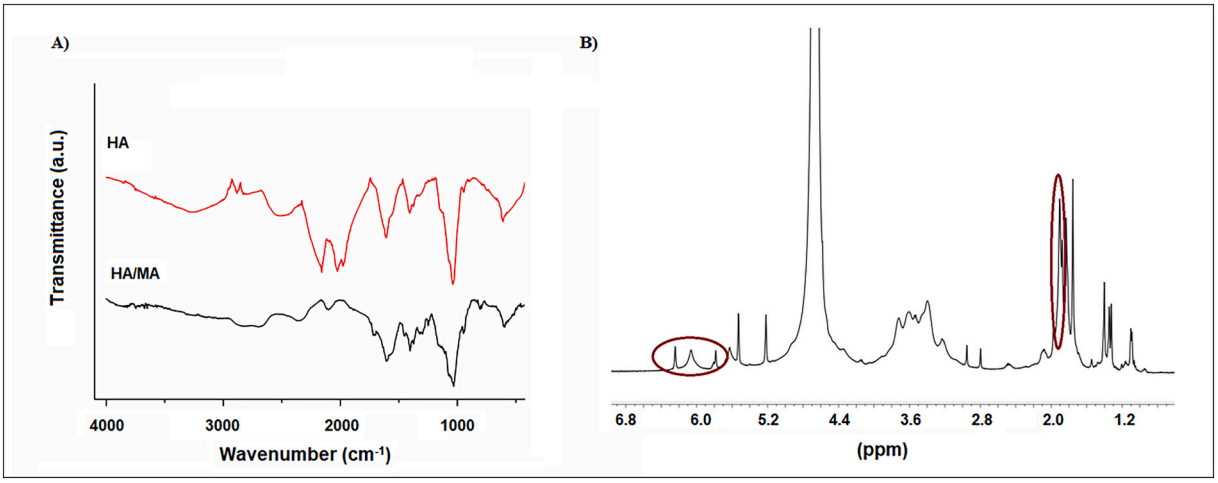

Fig. 2. FT-IR (A) spectra of HA and HA/MA and ^{1}H NMR (B) spectra of HA/MA.

Furthermore, it was observed that the second degradation has a maximum decomposition rate of 228 °C indicated degradation of the main polysaccharide backbone and the final degradation took place at nearly 392 °C due to the decomposition of polymeric side chains in the HA/MA-rGO hydrogel.

The TGA curve of the HA/MA-rGO-PANI hydrogel exhibited the first degradation in the temperature range of 150 and 190 °C due to loss of water molecules and the second degradation with a maximum rate at 216 °C assigned to the degradation of semi-interpenetrating hydrogel network. When the DTG curve of hydrogel including PANI was checked, it was clearly observed that HA/MA-rGO-PANI hydrogel showed a distinct separation of the peak appearing as a small shoulder in both

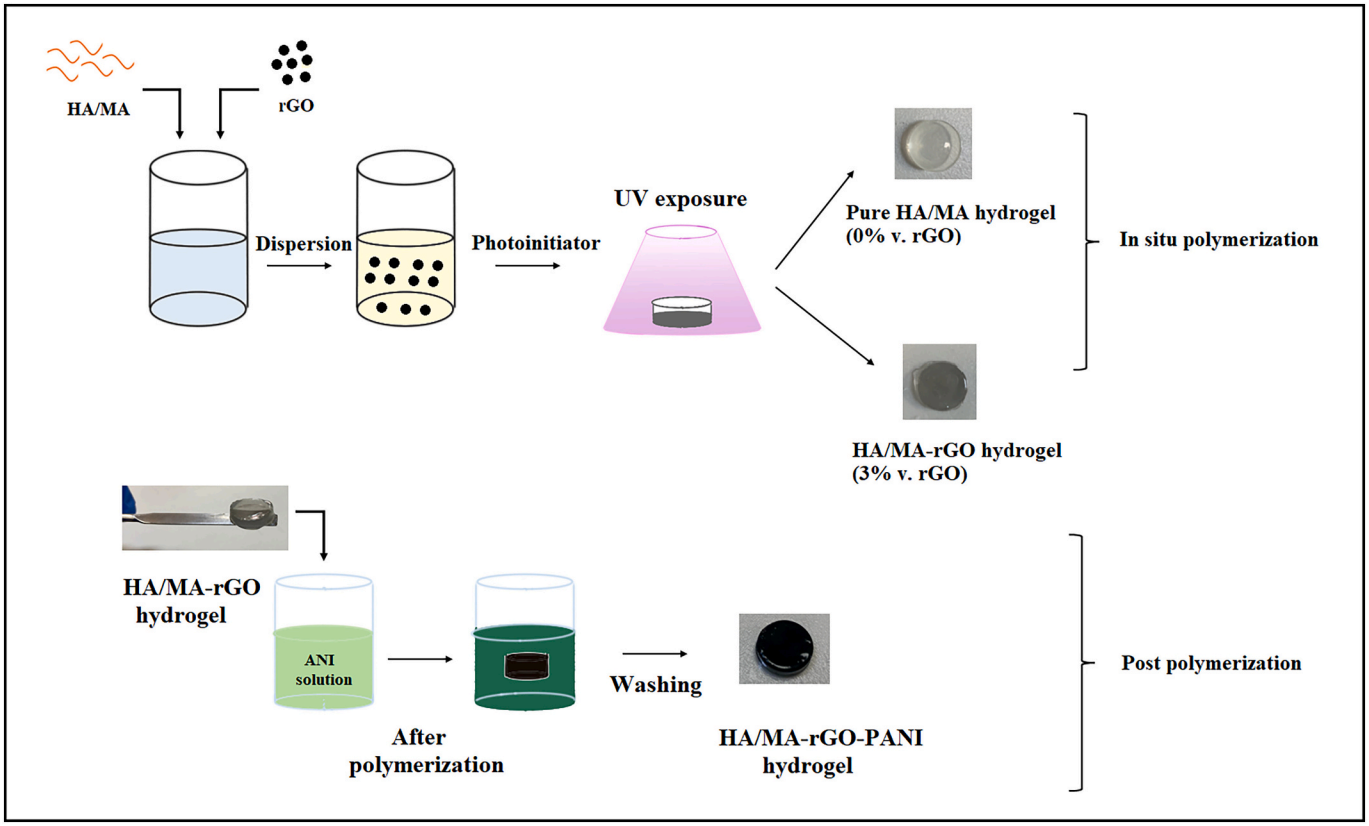

Scheme 2. Schematic representation of the production of HA/MA, HA/MA-rGO and HA/MA-rGO-PANI hydrogels.

DTG curves of HA/MA and HA/MA-rGO hydrogels. This single broad peak proved the attractive molecular interactions including $\pi - \pi$ and hydrogen bonding and a higher degree of compatibility of all components in the hydrogel network. The third weight loss occurred at a higher temperature for HA/MA-rGO-PANI hydrogel which is clear evidence for the improvement in thermal stability due to the thermal degradation resistance originating from the PANI structure [88].

3.5. Swelling properties

The swelling capacity is a key parameter for ECHs that shows their suitability for biomaterial applications such as sensor, drug delivery, tissue engineering and wound dressing applications where the transfer of molecules plays a significant role [47,89]. As the swelling behavior could be connected to several essential aspects of the hydrogels such as their morphology, permeability, toughness and biocompatibility, the evaluation of ECHs in terms of swelling properties is a necessity for their usage as a biomaterial [90,91]. To determine this important feature of the produced hydrogels, the swelling test was performed in PBS medium, of which physical and chemical properties are similar to human body fluid. As shown in Fig. 6A, while the swelling capacity of the HA/MA hydrogel was found as 684 %, the swelling ratio increased to 850 % after the incorporation of rGO into a polymeric network that could be explained by the presence of hydrophilic groups coming from rGO structure [92,93]. These hydrophilic functional groups could be simultaneously formed the hydrogen bonds with water molecules. Therefore, more water molecules were kept in the hydrogel structure resulted in the enhancement of the swelling ratio [94,95]. On the other hand, HA/MA-rGO-PANI hydrogel showed a considerable decrease in swelling capacity because of the rigid and more hydrophobic structure of PANI compared to HA/MA-rGO hydrogel network. This decrement could be also attributed to filling the voids of the hydrogel structure by PANI. Additionally, the electrostatic and molecular interactions between PANI and hydrogel network, which prevented the bonding of structure with water molecules, might be a possible reason for decreasing the swelling capacity [96,97].

3.6. Electrical conductivity

Since ECHs based on a natural-origin polymer could enhance intercellular and biological activity by mimicking extracellular matrix (ECM), they would be used as a promising alternative material for smart drug carriers [98,99]. Particularly, the production of ECHs with a reasonable level of conductivity offers enhanced performance and productivity in desired biomaterial applications [47]. Considering this, the electrical conductivity of HA/MA-PANI, HA/MA-rGO and HA/MA-rGO-PANI hydrogels was evaluated by measuring the sheet resistance values of them through the four-point probe method. All conductivity results were given as a table and graph (Table 2, Fig. 6B). Based on the results, it is clear that the conductivity of HA/MA-rGO-PANI hydrogel is superior to that of the HA/MA-only PANI and HA/MA-only rGO hydrogels. Because there is the important contribution of both RGO and PANI in the HA/MA-rGO-PANI hydrogel; i) the well-distributed rGO particles in the hydrogel network form the effective and conductive pathway leading to an electroconductive structure [100] ii) the polyconjugated planar structure of PANI provides electrical conductivity and the electron delocalization of polaron/bipolaron structures in the hydrogel network [88,101]. This significant enhancement in the conductivity proves that the integration of both rGO and PANI as different conductivity sources in the hydrogel structure supplies more sufficient electrical conductivity to the produced hydrogels.

3.7. Mechanical performance

The mechanical performance of the hydrogels employing for drug delivery systems is a highly significant parameter to provide an effective

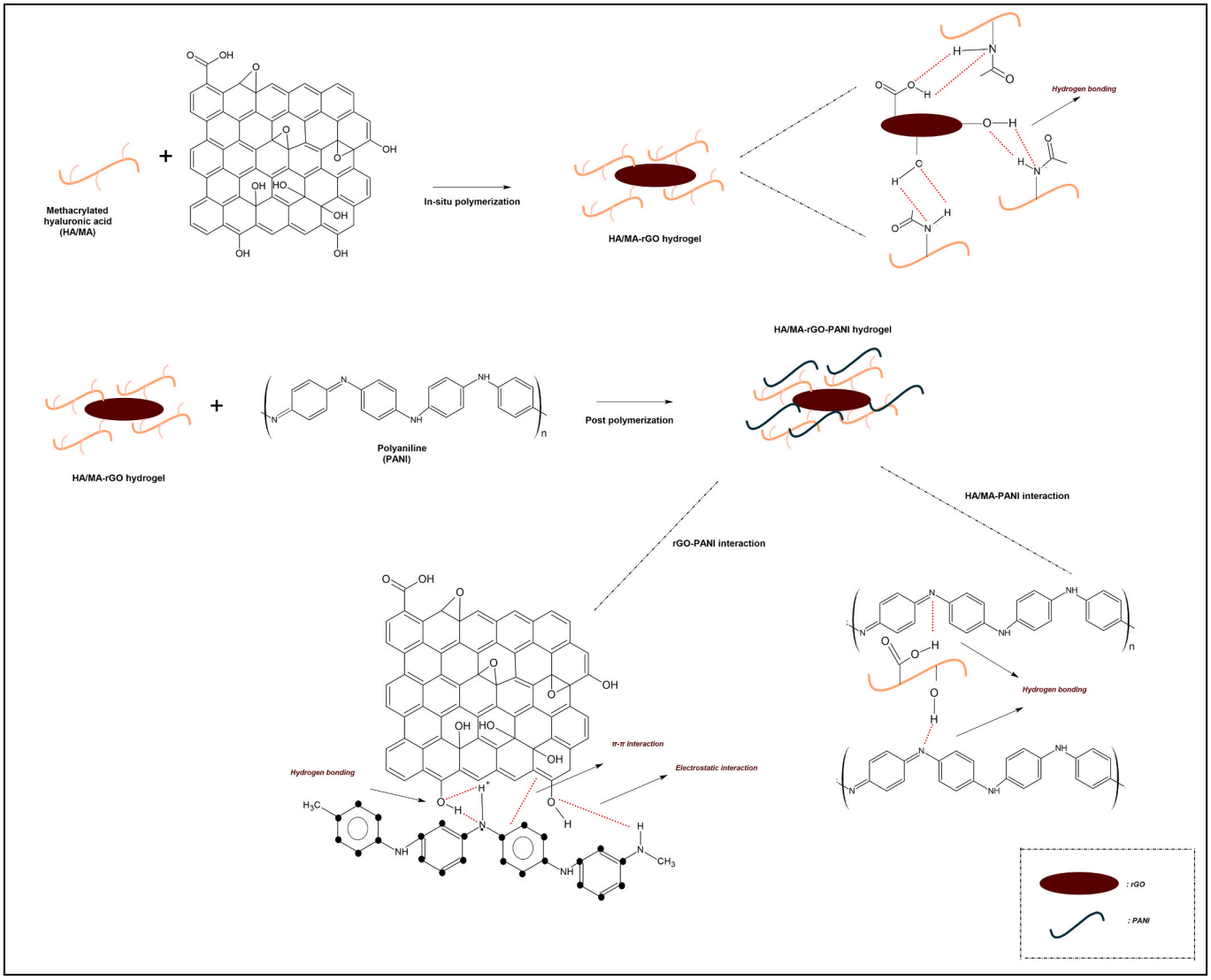

Scheme 3. Schematic representation of the plausible interactions of the components (HA/MA, rGO and PANI) in the hydrogel network.

protection for their structural integrity against external forces. Therefore, the mechanical properties of the produced hydrogels were analyzed to investigate their usage as a drug carrier in practical applications. Fig. 7 represents the compressive stress-strain curves of the HA/MA, HA/MA-rGO, and HA/MA-rGO-PANI hydrogels conducted at room temperature. As seen from these curves' the slopes showing elastic modulus, pure hydrogel (HA/MA) showed the lowest elastic modulus as well as the lowest elongation at break. Elastic modulus and compressive strength (the ultimate breaking strength) significantly increased in the presence of the rGO and PANI. Furthermore, the absence of free space owing to especially introduction of PANI into the polymeric network and uniform network into the hydrogel structure is to allow stress to be distributed uniformly and improves the mechanical properties [102].

Notably, it appears from the stress-strain curves that the presence of the rGO and PANI had significant influences on the toughness, the area under the stress-strain curve, of the obtained hydrogels and demonstrates the absorbed energy of the hydrogel up to the final rapture. Both rGO and PANI remarkably increased stress-strain performance since physical entanglements as well as inter-and intra-molecular hydrogen bonds between PANI, rGO and HA mainly account for strengthening the hydrogel [103].

The results regarding compressive strength and elastic modulus obtained from the stress-strain curve are listed in Table 3. The compressive strength of the hydrogel reached to 472.06 kPa with an enhanced elastic modulus of 5.77 kPa after the incorporation of rGO into HA/MA hydrogel network that could be attributed to the reinforcement effect of rGO. In particular, hydrogen bonding between rGO and polymeric network effectively promote the strength of the hydrogel resulted in the increment of their resistance ability to external forces. After post polymerization of PANI, while the compressive strength of the HA/MA-rGO hydrogel was increased nearly by double, the elastic modulus value of HA/MA-rGO-PANI hydrogel reached to 23.60 kPa indicated excellent flexibility, which was 4 times and 12 times higher than that of the HA/MA-rGO and HA/MA hydrogels, respectively. Such superior mechanical properties of HA/MA-rGO-PANI hydrogel could be explained by the rigid backbone of PANI as well as electrostatic interactions between PANI and the polymeric network. Furthermore, the formation of interpenetrated network could significantly strengthen the network structure. These results confirmed that the introduction of both rGO and PANI into hydrogel structure endowed outstanding mechanical performance to hydrogel comparing with HA/MA hydrogel, that is beneficial for their usage in drug release applications.

3.8. *In vitro degradation study*

In vitro degradation profile of HA/MA-rGO-PANI hydrogel in terms

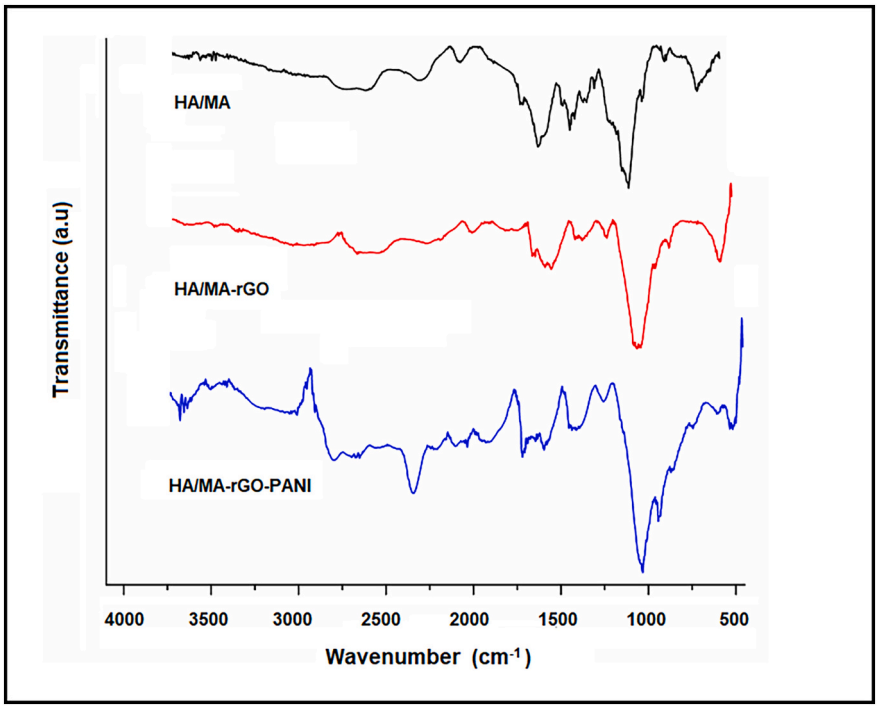

Fig. 3. FT-IR spectra of HA/MA, HA/MA-rGO and HA/MA-rGO-PANI hydrogels.

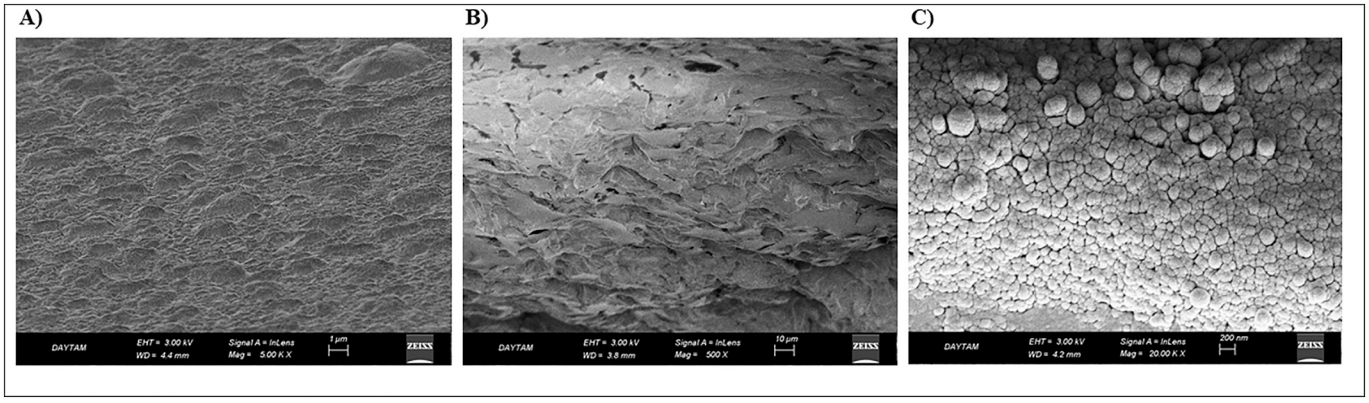

Fig. 4. SEM images of HA/MA (A) and HA/MA-rGO (B) and HA/MA-rGO-PANI (C) hydrogels.

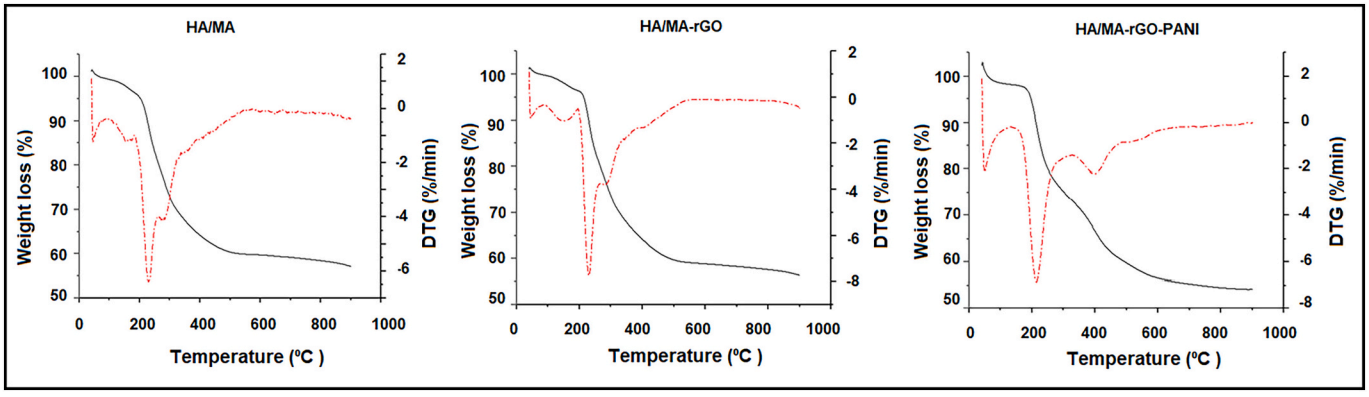

Fig. 5. TGA and DTG curves of HA/MA and HA/MA-rGO and HA/MA-rGO-PANI hydrogels.

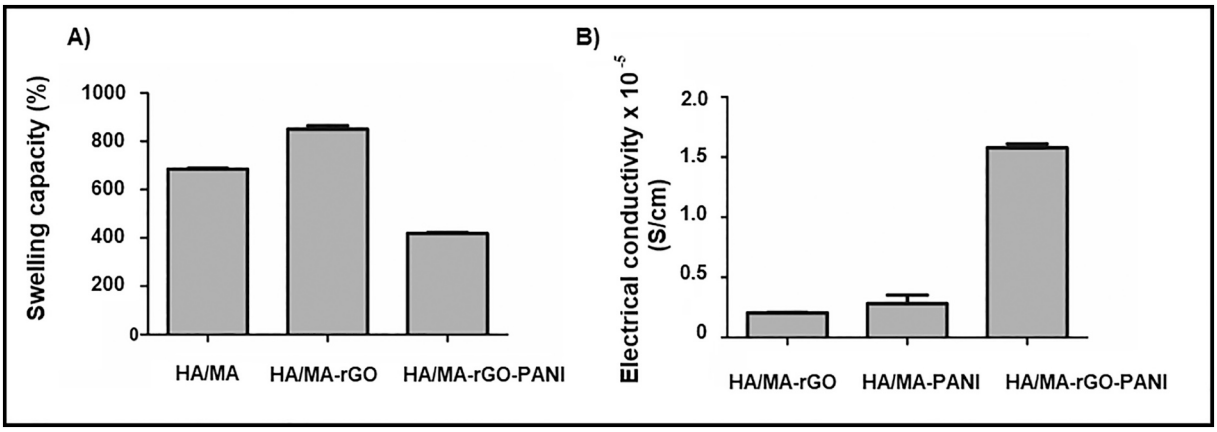

Fig. 6. Swelling capacity (A) and electrical conductivity (B) of the HA/MA, HA/MA-rGO and HA/MA-rGO-PANI hydrogels.

Table 2
Conductivity values of hydrogel samples.

Sample	Resistance (Ω)	Sheet resistivity (Ω. cm)	Conductivity (S/cm)	Average conductivity (S/cm)
HA/MA	NA	NA	NA	NA
HA/MA-rGO	62×10^4	4.94×10^5	2.02×10^{-6}	2.06×10^{-6}
	59×10^4	4.70×10^5	2.13×10^{-6}	
	62×10^4	4.94×10^5	2.02×10^{-6}	
HA/MA-PANI	30×10^4	2.39×10^5	4.18×10^{-6}	$2,83 \times 10^{-6}$
	50×10^4	3.99×10^5	2.51×10^{-6}	
	70×10^4	5.58×10^5	1.79×10^{-6}	
HA/MA-rGO-PANI	7.7×10^4	0.61×10^5	1.64×10^{-5}	1.58×10^{-5}
	8.1×10^4	0.64×10^5	1.56×10^{-5}	
	8.2×10^4	0.65×10^5	1.54×10^{-5}	

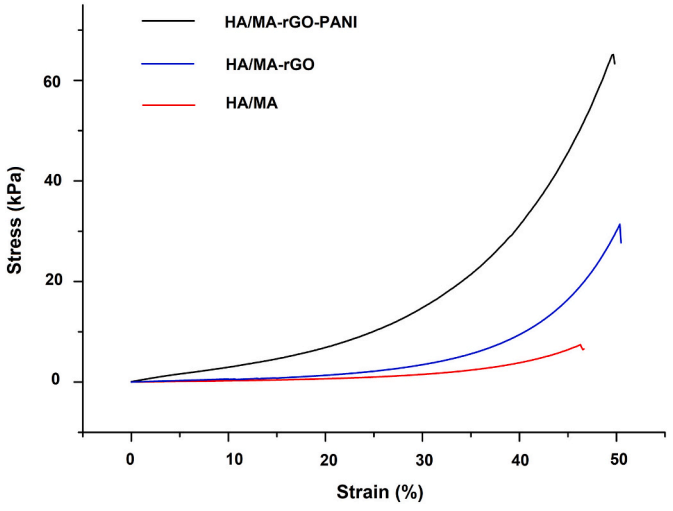

Fig. 7. Stress-strain curve of the HA/MA, HA/MA-rGO and HA/MA-rGO-PANI hydrogels.

Table 3
Mechanical properties of the produced hydrogels.

Sample	Compressive strength (kPa)	Elastic modulus (kPa)
HA/MA	191.79	1.86
HA/MA-rGO	472.06	5.77
HA/MA-rGO-PANI	992.11	23.60

of weight loss (%) was determined in PBS medium at 37 °C in order to mimic physiological conditions. The obtained results based on the day were given as a graph (Fig. 8A). As seen from the graph, the produced ECH exhibited only 27 % weight loss at the end of the 7th-day incubation. This result can be explained that while the breakage of glycosidic bonds in the polysaccharide component induces the degradation of the hydrogel network, PANI forms a barrier against water penetration due to its hydrophobic domain during the degradation period. The achieved slow degradation rate reveals that the fabricated HA/MA-rGO-PANI hydrogel would be able to preserve its integrity during the long period which is an essential requirement for some special implementations such as enduring drug treatment and neural implants.

3.9. Cytotoxicity test

The cytotoxicity of the HA/MA-rGO-PANI hydrogel was tested by proliferation of HaCaT cells seeded onto the hydrogel via MTS assay. As shown in Fig. 8B, there is no any significant difference between HA/MA-rGO-PANI hydrogel and control sample, which indicates that produced HA/MA-rGO-PANI hydrogel did not cause any cytotoxicity effect on the viability of HaCaT cells. Accordingly, it could be concluded that HA/MA-rGO-PANI hydrogel possessed sufficient cytocompatibility for controlled drug delivery applications.

3.10. Passive and electric-driven drug release studies

IBU, which is a hydrophobic anti-inflammatory reagent, was selected as the model drug for both passive and electric-driven drug release studies. The passive release behavior of the IBU (Fig. 9A) from the HA/MA-rGO-PANI hydrogel was investigated in PBS medium (pH 7.4) at 37 °C and the drug loading capacity of the hydrogel was found as % 57.8. The cumulative release percentage of the drug driven by the free diffusion mechanism reached to about 37 % at the end of 24 h. The rapid boost in the cumulative passive release at the initial stage ($t < 3$ min) was ascribed to the fast release of drug molecules weakly bounded to hydrogel or drugs presented near the surface of the hydrogel. After this initial stage, the IBU molecules were released in a slower and more controlled manner for 26 h. This behavior indicates that this hydrogel could be employed for controlled drug release applications.

Electric-driven release behavior of hydrogels which have favorable electrical conductive feature thanks to the integration of rGO and PANI into polymeric network was also tested by applying different voltage values (0 V, 1 V and 3 V) in order to evaluate the potential usage of HA/MA-rGO-PANI hydrogel as an electro-responsive drug carrier. As shown in Fig. 9B, the cumulative release of IBU significantly increased with the increment of applied voltage. While the cumulative release of IBU was approximately 35 % at the end of 140 min without electrical

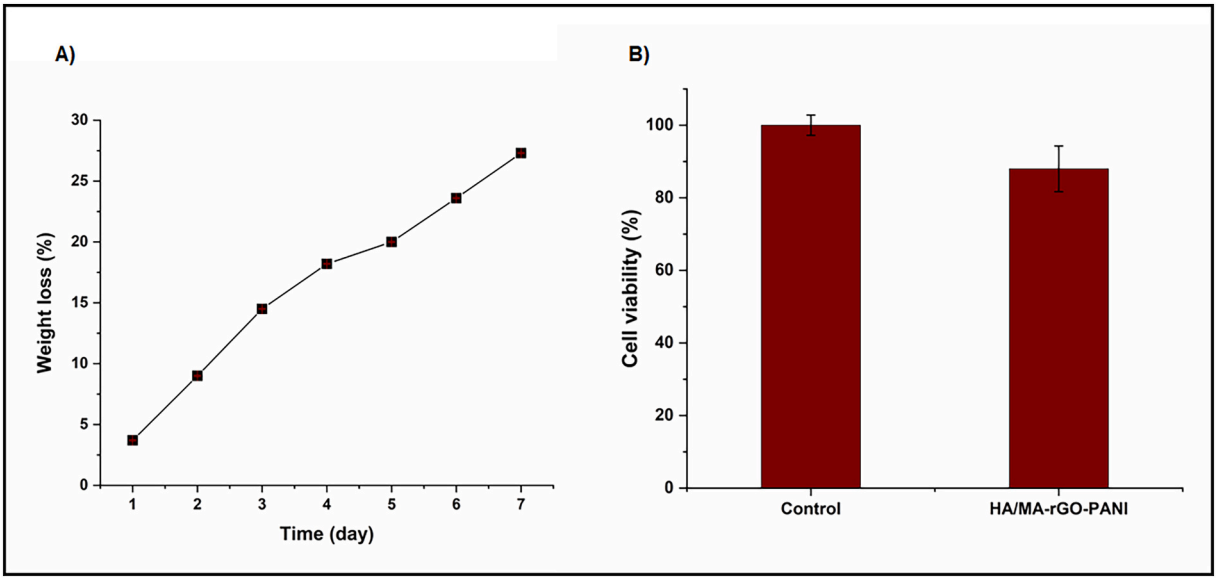

Fig. 8. In vitro degradation profile (A) and the cytotoxicity results (B) of the produced HA/MA-rGO-PANI hydrogel.

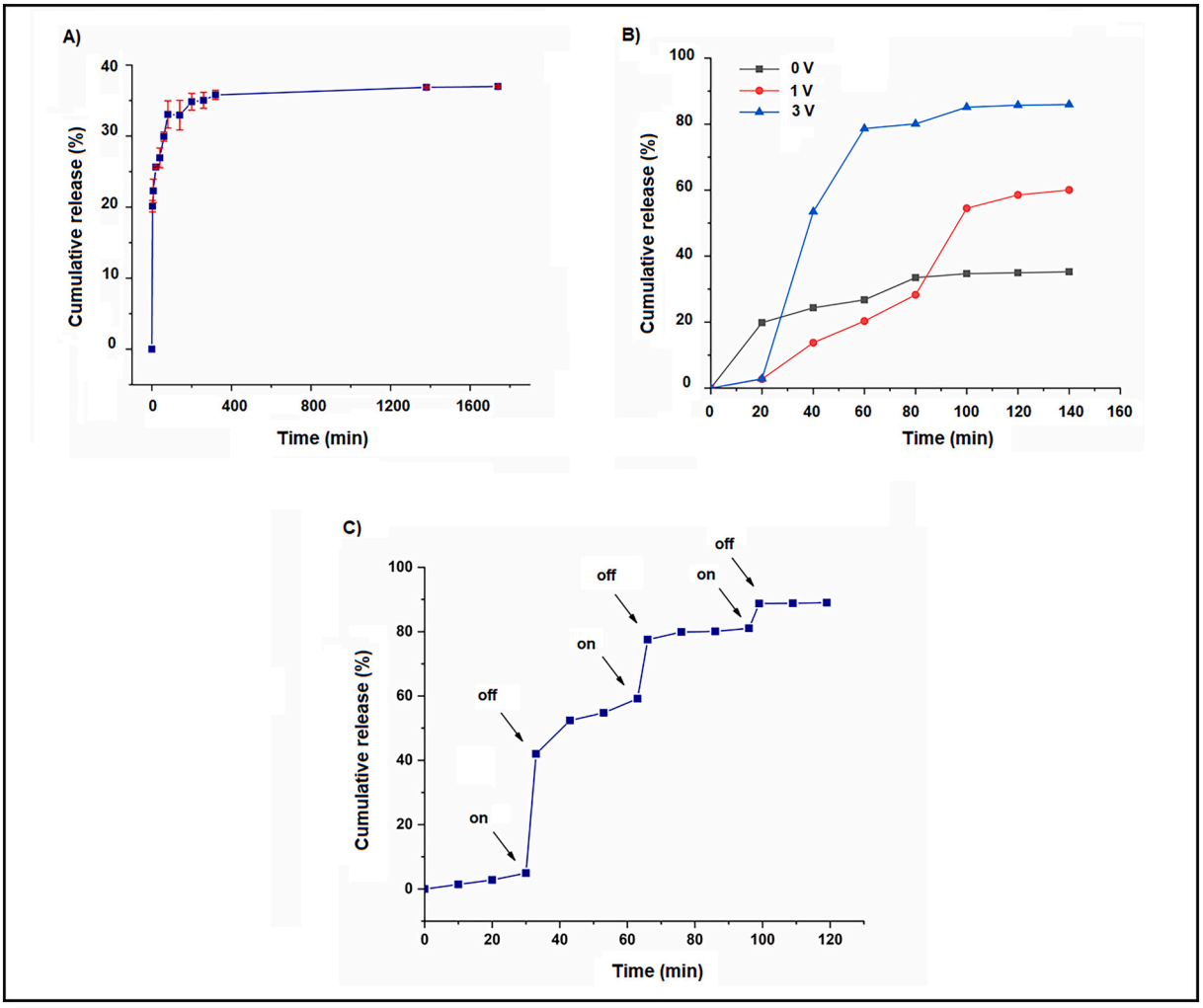

Fig. 9. Passive (A), electric-driven (B) and on-off pulse release behavior of IBU from HA/MA-rGO-PANI hydrogel.

stimulation, the cumulative release amounts of IBU were found as 60 % and 86 % at applied voltages of 1 V and 3 V, respectively. Since the dominant mechanism in the non-stimulated drug release is the free diffusion driven due to the concentration difference, the release of drug from the hydrogels occurred in slower manner resulted in lower cumulative release percentage [81]. On the other hand, electric-driven drug release from the hydrogels was induced by two mechanisms: (i) migration of charged molecules in the presence of electric field as a driving force and (ii) change of overall net charge within the polymeric network during the oxidation or reduction process [37,104]. In this study, a negatively charged drug (IBU) was loaded into hydrogel structure and it was released owing to the reduction of conductive polymer (PANI) into the fabricated ECH. By applying the electrical stimulation, the net positive charge in the hydrogel network was declined upon the reduction of PANI and negatively charged IBU molecules were expelled from the polymer matrix [1,3]. After that, charged moieties moved toward the electrode with an opposite charge by the driving force of electric field.

Furthermore, "on-off pulse" drug release was conducted at the voltage of 3 V for 3 min at 30 min intervals. While the loaded drug molecules were released slowly during the first 3 min without electrical stimulation, the release amount of IBU considerably increased with electrical stimulation during the subsequent 3 min. As shown in Fig. 9C, the first potential application enhanced the cumulative release of IBU from 5 % to 42 %.

A similar release pattern was also observed at the second and third on-off steps. The amount of cumulative drug release reached from 59 % to 77 % and from 81 % to 86 % in the second and third on-off steps, respectively. This decrement in the difference of cumulative release percentage could be explained by the reduction of drug concentration difference between polymeric matrix and PBS medium.

Both electric-stimuli and on-off pulse release behavior of the model drug verified the electro-responsive feature of fabricated HA/MA-rGO-PANI hydrogel and the utility of HA/MA-rGO-PANI as an anti-inflammatory reagent carrier in drug delivery systems.

4. Conclusion

Electroconductive hydrogels have become a remarkable platform for stimuli-responsive drug delivery applications, since the combination of outstanding properties of hydrogel structure and the electroactivity of the conductive components offer the novel perspectives for fabricating efficient ECH-based drug carrier systems. Herein, HA/MA-based ECHs were fabricated by using both in-situ polymerization with the incorporation of rGO into network and post polymerization of PANI. It should be noted that there are only a few reports on the usage of HA-based hydrogel as electro-responsive drug vehicles in the literature. Furthermore, the usage of both rGO and PANI as the different conductivity sources in HA-based polymeric network benefited from its polyelectrolyte nature for electrical-stimulated drug delivery applications was carried out for the first time in the current study. When the fabricated HA/MA-rGO-PANI hydrogel by this way was evaluated in terms of electroconductive and mechanical performance, it was obviously seen that the usage of two different approaches (in-situ and post polymerization) not only endowed efficient electrical conductivity (1.58×10^{-5} S/cm) to hydrogel but also provided improved mechanical performance in terms of compressive strength (992.11 kPa) and elastic modulus (23.60 kPa), which are the significant requirements for electric-driven drug release applications. More importantly, it was observed that the release of IBU from the hydrogels was stimulated by electrically and the cumulative release of the drug was also enhanced from 35 % (at 0 V) up to 86 % (at 3 V) with this stimulation during the release measurements. The achieved on-off pulse drug release pattern verified to possess an adequate level of electro-responsive ability of the hydrogel. All results showed that HA/MA-rGO-PANI hydrogel would be an attractive carrier for electro-responsive drug release systems that regulate drug release behavior according to the requirements of the patients in further neural implant applications.

CRediT authorship contribution statement

Didem Aycan: Methodology, Investigation, Visualization, Validation, Data curation, Writing – original draft, Writing – review & editing. **Fatma Karaca:** Resources, Project administration, Funding acquisition, Visualization. **Atıf Koca:** Methodology, Visualization, Resources. **Neslihan Alemdar:** Supervision, Conceptualization, Resources, Project administration, Methodology, Visualization, Validation, Data curation, Writing – original draft, Writing – review & editing.

Declaration of competing interest

The authors declare that they have no known competing financial interests or personal relationships that could have appeared to influence the work reported in this paper.

Data availability

Data will be made available on request.

Acknowledgments

The financial support for this study was granted by the Scientific Research Projects Commission (BAPKO) of Marmara University (Project no: FEN-C-DRP-130319-0073). We also thank Bilim Pharmaceuticals, Turkey for providing model drug (IBU).

References

[1] Z. Atoufi, P. Zarrintaj, G.H. Motlagh, A. Amiri, Z. Bagher, S.K. Kamrava, A novel bio electro active alginate-aniline tetramer/agarose scaffold for tissue engineering: synthesis, characterization, drug release and cell culture study, J. Biomater. Sci. Polym. Ed. 28 (15) (2017) 1617–1638.
[2] S. Ganguly, D. Ray, P. Das, P.P. Maity, S. Mondal, V. Aswal, S. Dhara, N.C. Das, Mechanically robust dual responsive water dispersible-graphene based conductive elastomeric hydrogel for tunable pulsatile drug release, Ultrason. Sonochem. 42 (2018) 212–227.
[3] J. Qu, X. Zhao, P.X. Ma, B. Guo, Injectable antibacterial conductive hydrogels with dual response to an electric field and pH for localized "smart" drug release, Acta Biomater. 72 (2018) 55–69.
[4] C.M. Wells, M. Harris, L. Choi, V.P. Murali, F.D. Guerra, J.A. Jennings, Stimuli-responsive drug release from smart polymers, J. Funct. Biomater. 10 (3) (2019) 34–53.
[5] Y. Yun, H. Wu, J. Gao, W. Dai, L. Deng, O. Lv, Y. Kong, Facile synthesis of Ca2+-crosslinked sodium alginate/graphene oxide hybrids as electro-and pH-responsive drug carrier, Mater. Sci. Eng. C 108 (2020) 110380–110385.
[6] I. Carayon, A. Gaubert, Y. Mousli, B. Philippe, Electro-responsive hydrogels: macromolecular and supramolecular approaches in the biomedical field, Biomater. Sci. 8 (20) (2020) 5589–5600.
[7] Z. Deng, Y. Guo, X. Zhao, P.X. Ma, B. Guo, Multifunctional stimuli-responsive hydrogels with self-healing, high conductivity, and rapid recovery through host–guest interactions, Chem. Mater. 30 (5) (2018) 1729–1742.
[8] N. Hosseini-Nassab, D. Samanta, Y. Abdolazimi, J.P. Annes, R.N. Zare, Electrically controlled release of insulin using polypyrrole nanoparticles, Nanoscale 9 (1) (2017) 143–149.
[9] Y. Wu, L. Wang, B. Guo, Y. Shao, P.X. Ma, Electroactive biodegradable polyurethane significantly enhanced schwann cells myelin gene expression and neurotrophin secretion for peripheral nerve tissue engineering, Biomaterials 87 (2016) 18–31.
[10] M. Bansal, A. Dravid, Z. Aqrawe, J. Montgomery, Z. Wu, D. Svirskis, Conducting polymer hydrogels for electrically responsive drug delivery, J. Control. Release 328 (2020) 192–209.
[11] S.S. Athukorala, T.S. Tran, R. Balu, V.K. Truong, J. Chapman, N.K. Dutta, N. Roy Choudhury, 3D printable electrically conductive hydrogel scaffolds for biomedical applications: a review, Polymers 13 (3) (2021) 474–497.
[12] K. Krukiewicz, P. Zawisza, A.P. Herman, R. Turczyn, S. Boncel, J.K. Zak, An electrically controlled drug delivery system based on conducting poly (3, 4-ethylenedioxypyrrole) matrix, Bioelectrochemistry 108 (2016) 13–20.
[13] A. Seyfoddin, A. Chan, W.-T. Chen, I. Rupenthal, G. Waterhouse, D. Svirskis, Electro-responsive macroporous polypyrrole scaffolds for triggered dexamethasone delivery, Eur. J. Pharm. Biopharm. 94 (2015) 419–426.

[14] Z. Aqrawe, J. Montgomery, J. Travas-Sejdic, D. Svirskis, Conducting polymers for neuronal microelectrode array recording and stimulation, Sens. Actuators B: Chem. 257 (2018) 753–765.
[15] J.A. Chikar, J.L. Hendricks, S.M. Richardson-Burns, Y. Raphael, B.E. Pfingst, D. C. Martin, The use of a dual PEDOT and RGD-functionalized alginate hydrogel coating to provide sustained drug delivery and improved cochlear implant function, Biomaterials 33 (7) (2012) 1982–1990.
[16] D. Svirskis, J. Travas-Sejdic, A. Rodgers, S. Garg, Electrochemically controlled drug delivery based on intrinsically conducting polymers, J. Control. Release 146 (1) (2010) 6–15.
[17] H. Yuk, B. Lu, X. Zhao, Hydrogel bioelectronics, Chem. Soc. Rev. 48 (6) (2019) 1642–1667.
[18] Y. Chen, K. Zheng, L. Niu, Y. Zhang, Y. Liu, C. Wang, F. Chu, Highly mechanical properties nanocomposite hydrogels with biorenewable lignin nanoparticles, Int. J. Biol. Macromol. 128 (2019) 414–420.
[19] R. Kulkarni, S. Biswanath, Electrically responsive smart hydrogels in drug delivery: a review, J. Appl. Biomater. Biomech. 5 (3) (2007) 125–139.
[20] J. Qu, Y. Liang, M. Shi, B. Guo, Y. Gao, Z. Yin, Biocompatible conductive hydrogels based on dextran and aniline trimer as electro-responsive drug delivery system for localized drug release, Int. J. Biol. Macromol. 140 (2019) 255–264.
[21] M.N. Sundaram, S. Amirthalingam, U. Mony, P.K. Varma, R. Jayakumar, Injectable chitosan-nano bioglass composite hemostatic hydrogel for effective bleeding control, Int. J. Biol. Macromol. 129 (2019) 936–943.
[22] N. Dubashynskaya, D. Poshina, S. Raik, A. Urtti, Y.A. Skorik, Polysaccharides in ocular drug delivery, Pharmaceutics 12 (1) (2019) 22–51.
[23] M.S. Hasnain, A.K. Nayak, Natural Polysaccharides in Drug Delivery and Biomedical Applications, Academic Press, 2019.
[24] P. Prasher, M. Sharma, M. Mehta, S. Satija, A.A. Aljabali, M.M. Tambuwala, K. Anand, N. Sharma, H. Dureja, N.K. Jha, Current-status and applications of polysaccharides in drug delivery systems, Colloid InterfaceSci.Commun. 42 (2021) 100418–100434.
[25] A. Puiggalí-Jou, E. Cazorla, G. Ruano, I. Babeli, M.-P. Ginebra, J. García-Torres, C. Alemán, Electroresponsive alginate-based hydrogels for controlled release of hydrophobic drugs, ACS Biomater. Sci. Eng. 6 (11) (2020) 6228–6240.
[26] A. Sood, A. Gupta, G. Agrawal, Recent advances in polysaccharides based biomaterials for drug delivery and tissue engineering applications, Carbohydr. Polym. Technol. Appl. 2 (2021) 100067–100090.
[27] H. Ge, Y. Kong, D. Shou, L. Deng, Communication—three-dimensional electro- and pH-responsive polypyrrole/alginate hybrid for dual-controlled drug delivery, J. Electrochem. Soc. 163 (5) (2016) G33–G36.
[28] R. Wang, D. Shou, O. Lv, Y. Kong, L. Deng, J. Shen, pH-controlled drug delivery with hybrid aerogel of chitosan, carboxymethyl cellulose and graphene oxide as the carrier, Int. J. Biol. Macromol. 103 (2017) 248–253.
[29] J. Xu, Y.-L. Tsai, S.-H. Hsu, Design strategies of conductive hydrogel for biomedical applications, Molecules 25 (22) (2020) 5296–5312.
[30] B.W. Walker, R.P. Lara, E. Mogadam, C.H. Yu, W. Kimball, N. Annabi, Rational design of microfabricated electroconductive hydrogels for biomedical applications, Prog. Polym. Sci. 92 (2019) 135–157.
[31] M. Wang, Y. Chen, R. Khan, H. Liu, C. Chen, T. Chen, R. Zhang, H. Li, A fast self-healing and conductive nanocomposite hydrogel as soft strain sensor, Colloids Surf. A Physicochem. Eng. Asp. 567 (2019) 139–149.
[32] X. Liu, Y. Ma, X. Zhang, J. Huang, Cellulose nanocrystal reinforced conductive nanocomposite hydrogel with fast self-healing and self-adhesive properties for human motion sensing, Colloids Surf. A Physicochem. Eng. Asp. 613 (2021) 126076–126085.
[33] S.R.U. Rehman, R. Augustine, A.A. Zahid, R. Ahmed, M. Tariq, A. Hasan, Reduced graphene oxide incorporated GelMA hydrogel promotes angiogenesis for wound healing applications, Int. J. Nanomedicine 14 (2019) 9603–9617.
[34] Y. Wang, F. Huang, X. Chen, X.-W. Wang, W.-B. Zhang, J. Peng, J. Li, M. Zhai, Stretchable, conductive, and self-healing hydrogel with super metal adhesion, Chem. Mater. 30 (13) (2018) 4289–4297.
[35] B. Abdi, R.C. Hendriks, A.-J. van der Veen, N.M. de Groot, A compact matrix model for atrial electrograms for tissue conductivity estimation, Comput. Biol. Med. 107 (2019) 284–291.
[36] C. Boehler, F. Oberueber, M. Asplund, Tuning drug delivery from conducting polymer films for accurately controlled release of charged molecules, J. Control. Release 304 (2019) 173–180.
[37] C. Pérez-Martínez, S.D.M. Chávez, T. del Castillo-Castro, T.E.L. Ceniceros, M. Castillo-Ortega, D. Rodríguez-Félix, J.C.G. Ruiz, Electroconductive nanocomposite hydrogel for pulsatile drug release, React. Funct. Polym. 100 (2016) 12–17.
[38] J.-G. Wu, J.-H. Chen, K.-T. Liu, S.-C. Luo, Engineering antifouling conducting polymers for modern biomedical applications, ACS Appl. Mater. Interfaces 11 (24) (2019) 21294–21307.
[39] S. Mondal, S. Das, A.K. Nandi, A review on recent advances in polymer and peptide hydrogels, Soft Matter 16 (6) (2020) 1404–1454.
[40] B. Tandon, A. Magaz, R. Balint, J.J. Blaker, S.H. Cartmell, Electroactive biomaterials: vehicles for controlled delivery of therapeutic agents for drug delivery and tissue regeneration, Adv. Drug Deliv. Rev. 129 (2018) 148–168.
[41] R. Alizadeh, P. Zarrintaj, S.K. Kamrava, Z. Bagher, M. Farhadi, F. Heidari, A. Komeili, T.J. Gutiérrez, M.R. Saeb, Conductive hydrogels based on agarose/alginate/chitosan for neural disorder therapy, Carbohydr. Polym. 224 (2019) 115161–115171.
[42] Z. Bagher, Z. Atoufi, R. Alizadeh, M. Farhadi, P. Zarrintaj, L. Moroni, M. Setayeshmehr, A. Komeili, S.K. Kamrava, Conductive hydrogel based on chitosan-aniline pentamer/gelatin/agarose significantly promoted motor neuron-like cells differentiation of human olfactory ecto-mesenchymal stem cells, Mater. Sci. Eng. C 101 (2019) 243–253.
[43] B. Bagheri, P. Zarrintaj, S.S. Surwase, N. Baheiraei, M.R. Saeb, M. Mozafari, Y. C. Kim, O.O. Park, Self-gelling electroactive hydrogels based on chitosan–aniline oligomers/agarose for neural tissue engineering with on-demand drug release, Colloids Surf. B: Biointerfaces 184 (2019) 110549–110558.
[44] S. Manouchehri, B. Bagheri, S.H. Rad, M.N. Nezhad, Y.C. Kim, O.O. Park, M. Farokhi, M. Jouyandeh, M.R. Ganjali, M.K. Yazdi, Electroactive bio-epoxy incorporated chitosan-oligoaniline as an advanced hydrogel coating for neural interfaces, Prog. Org. Coat. 131 (2019) 389–396.
[45] P. Zarrintaj, H. Vahabi, M.R. Saeb, M. Mozafari, Application of polyaniline and its derivatives, in: Fundamentals and Emerging Applications of Polyaniline, Elsevier, 2019, pp. 259–272.
[46] D.N. Heo, S.-J. Lee, R. Timsina, X. Qiu, N.J. Castro, L.G. Zhang, Development of 3D printable conductive hydrogel with crystallized PEDOT: PSS for neural tissue engineering, Mater. Sci. Eng. C 99 (2019) 582–590.
[47] C. Xu, S. Guan, S. Wang, W. Gong, T. Liu, X. Ma, C. Sun, Biodegradable and electroconductive poly(3,4-ethylenedioxythiophene)/carboxymethyl chitosan hydrogels for neural tissue engineering, Mater. Sci. Eng. C Mater. Biol. Appl. 84 (2018) 32–43.
[48] Y. Yang, L. Xu, J. Wang, Q. Meng, S. Zhong, Y. Gao, X. Cui, Recent advances in polysaccharide-based self-healing hydrogels for biomedical applications, Carbohydr. Polym. 283 (2022), 119161.
[49] D. Aycan, N. Dolapçı, Ö.G. Karaca, N. Alemdar, Polysaccharide-based electroconductive films for controlled release of ciprofloxacin, J. Appl. Polym. Sci. 139 (32) (2022), e52761.
[50] I.S. Bayer, Hyaluronic acid and controlled release: a review, Molecules 25 (11) (2020) 2649.
[51] S. Ganguly, P.P. Maity, S. Mondal, P. Das, P. Bhawal, S. Dhara, N.C. Das, Polysaccharide and poly (methacrylic acid) based biodegradable elastomeric biocompatible semi-IPN hydrogel for controlled drug delivery, Mater. Sci. Eng. C 92 (2018) 34–51.
[52] K. Sutani, I. Kaetsu, K. Uchida, The synthesis and the electric-responsiveness of hydrogels entrapping natural polyelectrolyte, Radiat. Phys. Chem. 61 (1) (2001) 49–54.
[53] S. Golde, A. Coles, J.A. Lindquist, A. Compston, Decreased iNOS synthesis mediates dexamethasone-induced protection of neurons from inflammatory injury in vitro, Eur. J. Neurosci. 18 (9) (2003) 2527–2537.
[54] R.A. Green, N.H. Lovell, L.A. Poole-Warren, Cell attachment functionality of bioactive conducting polymers for neural interfaces, Biomaterials 30 (22) (2009) 3637–3644.
[55] J. Li, Y. Wang, D. Ba, Characterization of semiconductor surface conductivity by using microscopic four-point probe technique, Phys. Procedia 32 (2012) 347–355.
[56] X. Liu, L. Xie, H. Li, Electrochemical biosensor based on reduced graphene oxide and au nanoparticles entrapped in chitosan/silica sol–gel hybrid membranes for determination of dopamine and uric acid, J. Electroanal. Chem. 682 (2012) 158–163.
[57] M. Yadav, S. Ahmad, Montmorillonite/graphene oxide/chitosan composite: synthesis, characterization and properties, Int. J. Biol. Macromol. 79 (2015) 923–933.
[58] B. Kartick, S.K. Srivastava, I. Srivastava, Green synthesis of graphene, J. Nanosci. Nanotechnol. 13 (6) (2013) 4320–4324.
[59] Y. Lin, J. Jin, M. Song, Preparation and characterisation of covalent polymer functionalized graphene oxide, J. Mater. Chem. 21 (10) (2011) 3455–3461.
[60] R.A. Rochman, S. Wahyuningsih, A.H. Ramelan, Q.A. Hanif, Preparation of nitrogen and sulphur co-doped reduced graphene oxide (rGO-NS) using N and S heteroatom of thiourea, IOP Conf.Ser.: Mater. Sci. Eng. 509 (2019), 012119.
[61] S. Thakur, N. Karak, Green reduction of graphene oxide by aqueous phytoextracts, Carbon 50 (14) (2012) 5331–5339.
[62] S. Narksitipan, S. Thongtem, Synthesis and characterization of transparent graphene oxide nanosheets, Ferroelectr. Lett. Sect. 41 (4–6) (2014) 94–99.
[63] L. Shahriary, A.A. Athawale, Graphene oxide synthesized by using modified hummers approach, Int. J. Renew. Energy Environ. Eng. 2 (01) (2014) 58–63.
[64] D. Konios, M.M. Stylianakis, E. Stratakis, E. Kymakis, Dispersion behaviour of graphene oxide and reduced graphene oxide, J. Colloid Interface Sci. 430 (2014) 108–112.
[65] Y. Zhu, M.D. Stoller, W. Cai, A. Velamakanni, R.D. Piner, D. Chen, R.S. Ruoff, Exfoliation of graphite oxide in propylene carbonate and thermal reduction of the resulting graphene oxide platelets, ACS Nano 4 (2) (2010) 1227–1233.
[66] M.J. Fernández-Merino, L. Guardia, J. Paredes, S. Villar-Rodil, P. Solís-Fernández, A. Martínez-Alonso, J. Tascón, Vitamin C is an ideal substitute for hydrazine in the reduction of graphene oxide suspensions, J. Phys. Chem. C 114 (14) (2010) 6426–6432.
[67] M. Mm, E.Sa Abo El, H. My, M. Ms, K. Mh, Thermally reduced graphene oxide: synthesis, structural and electrical properties, Int. J. Nanopart. Nanotechnol. 3 (1) (2017) 008.
[68] N. Alemdar, Fabrication of a novel bone ash-reinforced gelatin/alginate/hyaluronic acid composite film for controlled drug delivery, Carbohydr. Polym. 151 (2016) 1019–1026.
[69] D. Aycan, B. Selmi, E. Kelel, T. Yildirim, N. Alemdar, Conductive polymeric film loaded with IBUprofen as a wound dressing material, Eur. Polym. J. 121 (2019), 109308.
[70] C. Xia, P. Chen, S. Mei, L. Ning, C. Lei, J. Wang, J. Zhang, J. Ma, S. Fan, Photo-crosslinked HAMA hydrogel with cordycepin encapsulated chitosan microspheres for osteoarthritis treatment, Oncotarget 8 (2) (2017) 2835.

[71] L. He, J. Yang, J. Lu, Y. Xiao, Y. Fan, X. Zhang, Preparation and characterization of a novel hyaluronic acid–icariin conjugate hydrogel, Mater. Lett. 136 (2014) 41–44.
[72] K.K. Niloy, M. Gulfam, K.B. Compton, D. Li, G.T.J. Huang, T.L. Lowe, Methacrylated hyaluronic acid-based hydrogels maintain stemness in human dental pulp stem cells, Regen. Eng. Transl. Med. 6 (3) (2019) 262–272.
[73] J. Ryoo, J. Choi, C.S. Ki, Effect of ethanol treatment on physical property of photopolymerized hyaluronic acid/silk fibroin hybrid hydrogel, Polymer 202 (2020), 122733.
[74] V.T. Nguyen, N.T. Tran, T.L. Huynh, D.V.H. Le, D. Hoang, Reduced graphene oxide/cellulose microfiber hybrid from the Vietnamese Nipa palm tree: synthesis, properties, and applications for preparation of poly(methyl methacrylate) composite, J. Thermoplast. Compos. Mater. (2021) 1–21.
[75] M. Ates, M. Yildirim, The synthesis of rGO/RuO2, rGO/PANI, RuO2/PANI and rGO/RuO2/PANI nanocomposites and their supercapacitors, Polym. Bull. 77 (5) (2019) 2285–2307.
[76] M. Kalkan ErdoĞAn, M. SaÇAk, Electromagnetic shielding effectiveness of polyaniline/modified-poly(vinyl alcohol) film composite, Gazi Univ.J. Sci. 34 (2020) 381–394.
[77] I.L. Lera, S. Khasnabis, L.M. Wangatia, F.E. Olu, P.C. Ramamurthy, Insights into the electrochemical behavior and kinetics of NiP@PANI/rGO as a high-performance electrode for alkaline urea oxidation, Electrocatalysis 13 (3) (2022) 283–298.
[78] G. Yao, X. Liu, G. Zhang, Z. Han, H. Liu, Green synthesis of tannic acid functionalized graphene hydrogel to efficiently adsorb methylene blue, Colloids Surf. A Physicochem. Eng. Asp. 625 (2021), 126972.
[79] N. Sarkar, G. Sahoo, S.K. Swain, Reduced graphene oxide decorated superporous polyacrylamide based interpenetrating network hydrogel as dye adsorbent, Mater. Chem. Phys. 250 (2020), 123022.
[80] X.F. Song, J.T. Qin, T.T. Li, G. Liu, X.X. Xia, Y.S. Li, Y. Liu, Efficient construction and enriched selective adsorption-photocatalytic activity of PVA/PANI/TiO2 recyclable hydrogel by electron beam radiation, J. Appl. Polym. Sci. 137 (13) (2019) 48516.
[81] W. Li, X. Zeng, H. Wang, Q. Wang, Y. Yang, Polyaniline-poly (styrene sulfonate) conducting hydrogels reinforced by supramolecular nanofibers and used as drug carriers with electric-driven release, Eur. Polym. J. 66 (2015) 513–519.
[82] A. Słoniewska, B. Pałys, Supramolecular polyaniline hydrogel as a support for urease, Electrochim. Acta 126 (2014) 90–97.
[83] L. Zhang, M. Wan, Self-assembly of polyaniline—from nanotubes to hollow microspheres, Adv. Funct. Mater. 13 (10) (2003) 815–820.
[84] X. Fu, T. Li, F. Qi, S. Zhang, J. Wen, W. Shu, P. Luo, R. Zhang, S. Hu, Q. Liu, Designing high electrochemical surface area between polyaniline and hydrogel polymer electrolyte for flexible supercapacitors, Appl. Surf. Sci. 507 (2020), 145135.
[85] B.-J. Kim, S.-G. Oh, M.-G. Han, S.-S. Im, Preparation of polyaniline nanoparticles in micellar solutions as polymerization medium, Langmuir 16 (14) (2000) 5841–5845.
[86] J. Ma, J. Dai, Y. Duan, J. Zhang, L. Qiang, J. Xue, Fabrication of PANI-TiO2/rGO hybrid composites for enhanced photocatalysis of pollutant removal and hydrogen production, Renew.Energy 156 (2020) 1008–1018.
[87] M. Pieróg, M. Gierszewska-Drużyńska, J. Ostrowska-Czubenko, Effect of ionic crosslinking agents on swelling behavior of chitosan hydrogel membranes, Prog. Chem. Appl. Chitin Deriv. 75 (82) (2009) 3.
[88] S. Das, D.P. Chatterjee, A.K. Nandi, Supramolecular assembly of polythiophene-g-polymethacrylic acid-doped polyaniline with interesting morphological and opto-electronic properties, J. Mater. Chem. A 2 (30) (2014) 12031–12042.
[89] N. Cengiz, Fabrication of multifunctional stimuli-responsive hydrogels susceptible to both pH and metal cation for visual detections, Macromol. Chem. Phys. 220 (17) (2019), 1900212.
[90] H. Park, X. Guo, J.S. Temenoff, Y. Tabata, A.I. Caplan, F.K. Kasper, A.G. Mikos, Effect of swelling ratio of injectable hydrogel composites on chondrogenic differentiation of encapsulated rabbit marrow mesenchymal stem cells in vitro, Biomacromolecules 10 (3) (2009) 541–546.
[91] H. Zhang, C. Zhao, H. Cao, G. Wang, L. Song, G. Niu, H. Yang, J. Ma, S. Zhu, Hyperbranched poly (amine-ester) based hydrogels for controlled multi-drug release in combination chemotherapy, Biomaterials 31 (20) (2010) 5445–5454.
[92] S. Ghorbanzadeh Sheish, R. Emadi, M. Ahmadian, S. Sadeghzade, F. Tavangarian, Fabrication and characterization of polyvinylpyrrolidone-eggshell membrane-reduced graphene oxide nanofibers for tissue engineering applications, Polymers 13 (6) (2021) 913.
[93] B. Sharma, S. Thakur, D. Trache, H. Yazdani Nezhad, V.K. Thakur, Microwave-assisted rapid synthesis of reduced graphene oxide-based gum tragacanth hydrogel nanocomposite for heavy metal ions adsorption, Nanomaterials (Basel) 10 (8) (2020) 1616.
[94] L. Sánchez-Abella, V. Ruiz, A. Pérez-San Vicente, H.-J. Grande, I. Loinaz, D. Dupin, Reactive oxygen species (ROS)-responsive biocompatible polyethylene glycol nanocomposite hydrogels with different graphene derivatives, J. Mater. Sci. 56 (16) (2021) 10041–10052.
[95] T.Y. Tsai, K.H. Shen, C.W. Chang, L. Jovanska, R. Wang, Y.C. Yeh, In situ formation of nanocomposite double-network hydrogels with shear-thinning and self-healing properties, Biomater. Sci. 9 (3) (2021) 985–999.
[96] B. Bagheri, P. Zarrintaj, S.S. Surwase, N. Baheiraei, M.R. Saeb, M. Mozafari, Y. C. Kim, O.O. Park, Self-gelling electroactive hydrogels based on chitosan-aniline oligomers/agarose for neural tissue engineering with on-demand drug release, Colloids Surf. B Biointerfaces 184 (2019), 110549.
[97] D.O. Miranda, M.F. Dorneles, R.L. Oréfice, One-step process for the preparation of fast-response soft actuators based on electrospun hybrid hydrogel nanofibers obtained by reactive electrospinning with in situ synthesis of conjugated polymers, Polymer 200 (2020), 122550.
[98] B. Guo, J. Qu, X. Zhao, M. Zhang, Degradable conductive self-healing hydrogels based on dextran-graft-tetraaniline and N-carboxyethyl chitosan as injectable carriers for myoblast cell therapy and muscle regeneration, Acta Biomater. 84 (2019) 180–193.
[99] J. Liu, F. Cheng, H. Grénman, S. Spoljaric, J. Seppälä, J.E. Eriksson, S. Willför, C. Xu, Development of nanocellulose scaffolds with tunable structures to support 3D cell culture, Carbohydr. Polym. 148 (2016) 259–271.
[100] D. Kaya, N. Alemdar, Electroconductive hyaluronic acid/gelatin/poly(ethylene oxide) polymeric film reinforced by reduced graphene oxide, J. Appl. Polym. Sci. 136 (1) (2019) 46905.
[101] M.U. Celik, S. Ekici, Polyacrylamide-polyaniline composites: the effect of crosslinking on thermal, swelling, porosity, crystallinity, and conductivity properties, Colloid Polym. Sci. 297 (10) (2019) 1331–1343.
[102] S. Lee, H. Lee, J.H. Sim, D. Sohn, Graphene oxide/poly (acrylic acid) hydrogel by γ-ray pre-irradiation on graphene oxide surface, Macromol. Res. 22 (2) (2014) 165–172.
[103] Z. Liu, C. Zhang, H. Xu, X. Ma, Z. Shi, J. Yin, A facile method synthesizing hydrogel using hybranched polyether amine (hPEA) as coinitiator and crosslinker, Macromol. Chem. Phys. 218 (21) (2017) 1700251.
[104] J. Ge, E. Neofytou, T.J. Cahill III, R.E. Beygui, R.N. Zare, Drug release from electric-field-responsive nanoparticles, ACS Nano 6 (1) (2012) 227–233.